MIT Libraries | DSpace@MIT

MIT Open Access Articles

Extending Horsetail Matching for Optimization Under Probabilistic, Interval, and Mixed Uncertainties

The MIT Faculty has made this article openly available. ***Please share*** how this access benefits you. Your story matters.

Citation: Cook, Laurence W., et al. "Extending Horsetail Matching for Optimization Under Probabilistic, Interval, and Mixed Uncertainties." AIAA Journal, vol. 56, no. 2, Feb. 2018, pp. 849–61.

As Published: http://dx.doi.org/10.2514/1.J056371

Publisher: American Institute of Aeronautics and Astronautics (AIAA)

Persistent URL: http://hdl.handle.net/1721.1/116635

Version: Author's final manuscript: final author's manuscript post peer review, without publisher's formatting or copy editing

Terms of use: Creative Commons Attribution-Noncommercial-Share Alike

Massachusetts Institute of Technology

Extending Horsetail Matching for Optimization Under Probabilistic, Interval and Mixed Uncertainties

Laurence W. Cook*, Jerome P. Jarrett†
University of Cambridge, Cambridge, England, CB21PZ
Karen E. Willcox‡
Massachusetts Institute of Technology, Cambridge, Massachusetts, USA, 02139

This paper presents a new approach for optimization under uncertainty in the presence of probabilistic, interval and mixed uncertainties, avoiding the need to specify probability distributions on uncertain parameters when such information is not readily available. Existing approaches for optimization under these types of uncertainty mostly rely on treating combinations of statistical moments as separate objectives, but this can give rise to stochastically dominated designs. Here, horsetail matching is extended for use with these types of uncertainties to overcome some of the limitations of existing approaches. The formulation delivers a single, differentiable metric as the objective function for optimization. It is demonstrated on algebraic test problems, the design of a wing using a low-fidelity coupled aero-structural code, and the aerodynamic shape optimization of a wing using computational fluid dynamics analysis.

This is the authors' pre-print version. The published version is located at the following DOI: 10.2514/1.J056371, and was published online in AIAA Journal on 11th October 2017. Copyright 2017 Laurence W. Cook, Jerome P. Jarrett, Karen E. Willcox.

I. Introduction

Optimization techniques are becoming increasingly integrated within the design process of complex aerospace systems when a computational simulation of the system is available. Traditionally, an optimization minimizes a quantity of interest of a system (e.g., efficiency, cost, weight) as a function of controllable design variables, subject to some constraints. However, in practical problems, the computational simulation of the system will be subject to uncontrollable uncertainties from a variety of sources [1,2]. Ignoring the effect of these uncertainties on the quantity of interest in an optimization can give designs that lie in extreme regions of design space and see degraded performance when realized [3,4]. Therefore effective computational methods of handling uncertainties within the optimization process are needed; this is addressed by the field of optimization under uncertainty (OUU) [1].

Performing optimization under uncertainty requires that the uncertainties be represented mathematically. A typical approach is to treat uncertain parameters as random variables and to assign them probability distributions. However often the appropriate probability distribution to assign to the uncertain parameters is unknown, and so instead interval analysis can be used. Using intervals avoids imposing structure on the uncertainties that is unknown in reality and that can lead to erroneous levels of uncertainty on the output [5]. In general problems, both probabilistic and interval uncertainties can be present and so uncertainty quantification for mixed uncertainties has been developed [6–8].

This poses the question of how to use this mixed uncertainty information within an optimization. Existing approaches for design using optimization under mixed uncertainties are few: most examples to date use a weighted sum combination of average statistical moments and intervals of statistical moments [9–12]. However, such a formulation does not necessarily represent the goal of OUU (this is discussed further in Section II:B), and so in this work we develop an approach to optimization under mixed probabilistic and interval uncertainties that overcomes some of the limitations of the current state-of-the-art. Our approach builds on horsetail matching, a recent approach for optimization under probabilistic uncertainties, by extending the formulation and developing a numerical implementation that delivers a single, differentiable objective function for optimization under mixed uncertainties.

In Section II, the relevant background in mixed uncertainties and OUU is outlined. In Section III the concept of horsetail matching for mixed uncertainties is presented, the advantages of the approach compared to existing methods are discussed, and the numerical implementation is outlined. In Section IV, the effectiveness of the implementation is demonstrated. In Section V horsetail matching is applied to the low-fidelity aero-structural optimization of a wing and

*PhD Student, Department of Engineering. AIAA Student Member, lwc24@cam.ac.uk
†University Lecturer, Department of Engineering. AIAA Senior Member, jpj1001@cam.ac.uk
‡Professor, Department of Aeronautics and Astronautics. AIAA Associate Fellow, kwillcox@mit.edu

is compared to alternative optimization approaches. In Section VI it is applied to the aerodynamic shape optimization of a transonic wing analyzed using a 3D CFD RANS solver. Finally Section VII concludes the paper and proposes future work.

II. Background

We denote the quantity of interest that is being optimized as q, and the vector of controllable design variables as $\boldsymbol{x}$. The vectors $\boldsymbol{x}^L$ and $\boldsymbol{x}^U$ are respectively the vectors of upper and lower bounds on $\boldsymbol{x}$; along with the n_g inequality constraints $g_j(\boldsymbol{x}) \leq 0$ they define the set $\mathcal{X}$ that is the design space: $\mathcal{X} := \{\boldsymbol{x} \in \mathbb{R}^{n_x} \mid x_k^l < x_k < x_k^u \; \forall \; k = 1, ..., n_x \text{ and } g_j(\boldsymbol{x}) \leq 0 \; \forall \; j = 1, ..., n_g\}$. Input uncertainties in the problem are represented by a finite number of uncertain parameters which are given by the vector $\boldsymbol{u} \in \mathcal{U}$, such that each entry in $\boldsymbol{u}$ is an uncertain parameter that can be assigned either a probability distribution or an interval, and $\mathcal{U}$ is the set of values the uncertain parameters can take. The uncertain parameters in $\boldsymbol{u}$ that are treated probabilistically are denoted by $\boldsymbol{\theta}$, and those that are treated with interval analysis by $\boldsymbol{\phi}$; the quantity of interest q is thus a function of the design variables as well as these uncertain parameters: $q = q(\boldsymbol{x}, \boldsymbol{\theta}, \boldsymbol{\phi}) \in \mathcal{Q}$, where $\mathcal{Q}$ is the set of all feasible values of q.

A. Mixed Uncertainty Quantification

Treating an uncertain parameter as probabilistic requires that one assigns a probability distribution, whereas treating an uncertain parameter using interval analysis asserts that nothing more is known except that it lies between two values. One interpretation of this interval analysis is that the uncertain parameter is a random variable whose probability distribution could be any distribution that is bounded by the interval. When a mix of probabilistic and interval uncertainties are present in a problem, the result of a mixed uncertainty quantification analysis gives an ensemble of cumulative distribution functions (CDFs) over the range of the interval uncertain parameters; the envelope gives the interval at every probability level and the upper and lower bounds on the true CDF [6,7]. This uncertainty information is illustrated in Figure 1 (where a small subset of infinite possible CDFs are plotted), and is referred to as a "horsetail plot" (also known as a probability box, or p-box). Note that we use the term horsetail plot to refer to the two curves that give the upper and lower bounds on the CDF, not the entire ensemble of possible CDFs.

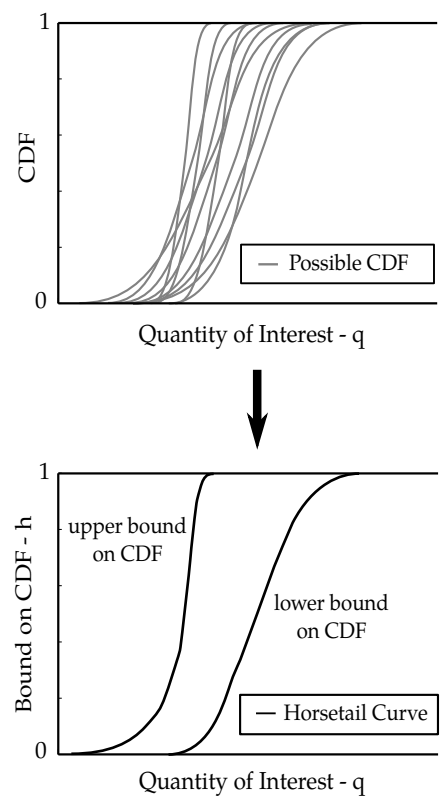

Figure 1: Example of a horsetail plot - the envelope of possible CDFs giving the two horsetail curves that represent the upper and lower bounds on the true CDF.

Other methods of propagating uncertainties beyond just probability and intervals are available, such as the Dempster-Shafer theory of evidence [13], and possibility theory [14]. These methods also result in a horsetail plot, in that they give upper and lower bounds on the true CDF of the quantity of interest. A horsetail plot is thus a rather general form of the output of an uncertainty analysis. A probabilistic analysis yields a special case of a horsetail plot where the upper and lower bounds on the CDF coincide. A purely interval based analysis yields another special case where the bounds are step functions.

The following definition of a horsetail plot is used in this paper (where the functions F_u and F_l are referred to as the horsetail curves):

Definition II.1. A horsetail plot consists of two non-decreasing functions $F_u \colon \mathcal{Q} \to [0,1]$ and $F_l \colon \mathcal{Q} \to [0,1]$ that represent the upper and lower bounds on the CDF respectively, where $\mathcal{Q}$ is the set of all possible values of the quantity of interest q.

B. Existing Approaches for Optimization Under Uncertainty

Handling uncertainties in optimization is not a challenge unique to engineering design, and has been considered extensively in other contexts. Often, such as in the field of operations research, "robust optimization" refers to optimizing under uncertain parameters that are contained in an uncertainty set, such that constraint satisfaction is guaranteed and the worst case of q is optimized [15, 16]. Using this formulation, known as the "robust counterpart", it is possible to preserve structure of the original problem, such as convexity. Alternatively "stochastic programming" refers to optimization under probabilistic uncertainties [17], where formulations that preserve structure of the problem have also been developed, such as by formulating the OUU problem using coherent risk measures [18].

Engineering design considers a broad range of problems that often lack the mathematical structure exploited in operations research (e.g., engineering design problems are typically non-convex, and in many cases the underlying analysis codes may be black box). Therefore, the development of OUU methods for engineering design has tended to focus on general-purpose optimization strategies that do not rely on specific problem structure [1]. Much of the previous work into OUU in aerospace design applications has considered exclusively probabilistic uncertainties where commonly the first two statistical moments of q (namely mean and variance) are considered in an optimization. These moments can be optimized separately in a multi-objective formulation [19, 20], or can be combined into a single objective using a weighted sum approach [21–24]. Various other methods for OUU have also been developed [1]. A notable alternative to statistical moment based methods is the "robust regularization" approach [1, 25], which is a minimax strategy optimizing the worst case performance over the uncertainty space, and so is comparable to the "robust counterpart" formulation of Ref. 16.

Most examples of design using optimization under mixed uncertainties to date use a weighted sum combination of average statistical moments and intervals of statistical moments [9–12]. For example, a common choice is

$$f_{obj} = w_1\bar{\mu} + w_2\bar{\sigma} + w_3\delta\mu \tag{1}$$

where f_{obj} is the objective function to be minimized, $\bar{\mu}$ is the midpoint of the interval of the means of possible CDFs, $\bar{\sigma}$ is the midpoint of the interval of standard deviations, $\delta\mu$ is the range of the interval of possible means, and w_1, w_2, w_3 are weights specified by the designer. Another suggested approach for robust design under mixed uncertainties is to minimize the interval of the 50% quantile [7].

Both in the probabilistic case and the mixed case, relying on statistical moments in the formulation of an optimization under uncertainty can give rise to stochastically dominated designs. Stochastic dominance indicates that for any given value of the quantity of interest q, a dominated design is less likely to obtain this value or better than another design [26]; this is a concept the authors argue is often overlooked in the engineering OUU literature. Stochastic dominance under probabilistic uncertainties is illustrated in Figure 2, and we use Definition II.2; it essentially means that the CDFs for the designs do not cross at any point.

Definition II.2. A design x_A *stochastically dominates* a design x_B (or design x_B is *stochastically dominated by* design x_A) under *probabilistic* uncertainties if

$$\forall q \in \mathcal{Q},\ F(q)_{x_A} > F(q)_{x_B}$$

or equivalently

$$\forall h \in [0,1],\ F^{-1}(h)_{x_A} < F^{-1}(h)_{x_B}$$

where $F(q)_x \colon \mathcal{Q} \to [0,1]$ and $F^{-1}(h)_x \colon [0,1] \to \mathcal{Q}$ are respectively the CDF and inverse CDF for design x.

The concept of stochastic dominance extends straightforwardly to mixed uncertainties, by defining it as when each horsetail curve for a design stochastically dominates the corresponding curve for another design according to Definition II.2. This is illustrated in Figure 2 and defined in Definition II.3:

Definition II.3. A design x_A *stochastically dominates* a design x_B (or design x_B is *stochastically dominated by* design x_A) under *mixed* uncertainties if

$$\forall q \in Q,\ F_u(q)_{x_A} > F_u(q)_{x_B} \text{ AND } F_l(q)_{x_A} > F_l(q)_{x_B}$$

or equivalently:

$$\forall h \in [0,1],\ F_u^{-1}(h)_{x_A} < F_u^{-1}(h)_{x_B} \text{ AND } F_l^{-1}(h)_{x_A} < F_l^{-1}(h)_{x_B}$$

where F_u and $F_l \colon Q \to [0,1]$ are respectively the upper and lower bound of the CDF, and F_u^{-1} and $F_l^{-1} \colon [0,1] \to Q$ are respectively the corresponding inverses.

Stochastic dominance under mixed uncertainties means that for any value of q, the bounds on the probability that a dominating design will achieve this performance or better are strictly higher than the dominated design.

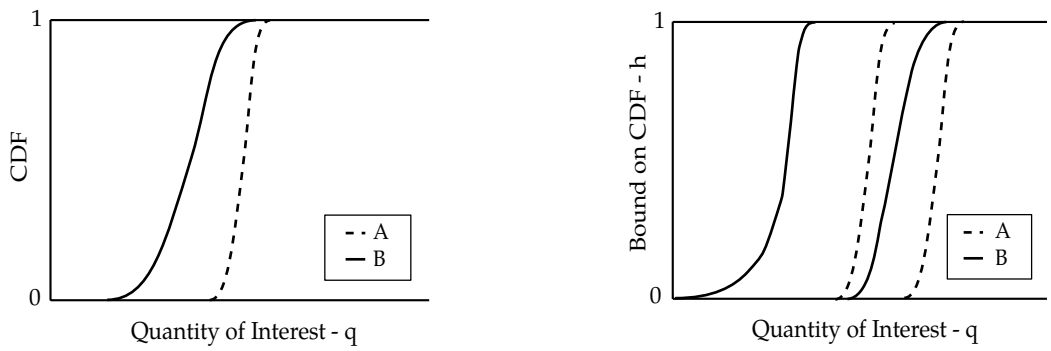

(a) Stochastic dominance under probabilistic uncertainties

(b) Stochastic dominance under mixed uncertainties

Figure 2: Stochastic dominance under probabilistic and mixed uncertainties. In both cases design x_A is stochastically dominated by design x_B, according to definitions II.2 and II.3.

Our design under uncertainty philosophy is built on the goal of maximizing the likelihood of achieving as good performance as possible. A stochastically dominated design is less likely to achieve a given value of q or better than another design, and thus the dominated design is considered objectively worse than the dominating design under this design philosophy. Treating combinations of statistical moments such as $\bar{\mu}$, $\bar{\sigma}$, and $\delta\mu$ as separate objectives in an optimization does not consider the possibility of obtaining stochastically dominated designs. Therefore, for some design problems, many of the designs on a Pareto front trading off $\bar{\mu}$, $\bar{\sigma}$, and $\delta\mu$ will be stochastically dominated by other designs and computational effort has been wasted obtaining them. Similarly if a weighted sum of these objectives is being optimized, some combinations of weightings will give rise to stochastically dominated designs. Since it is difficult to know *a priori* where on the Pareto front a given set of weightings will end up, this is a limitation of optimizing under mixed uncertainties using combinations of statistical moments. These arguments motivate the development of an alternative approach for optimization under mixed uncertainties.

III. Horsetail Matching

This section defines the difference metric underlying horsetail matching for mixed uncertainties, discusses its flexibility and describes its implementation. A python package that implements horsetail matching is freely available at *http://www-edc.eng.cam.ac.uk/aerotools/horsetailmatching*.

A. The Difference Metric

The concept of horsetail matching is to minimize the difference between the horsetail plot of the current design and a target, as illustrated in Figure 3. This extends the probabilistic case in [27] where the difference between a CDF and a target was minimized.

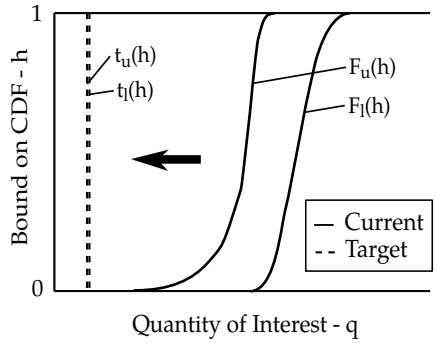

Figure 3: The horsetail matching concept: minimizing the difference between the horsetail plot of the quantity of interest q for the current design and a target. Adapted from [27].

The measure of this difference is given by the following horsetail matching metric:

$$d_{hm}(\boldsymbol{x}) = \Big(\int_0^1 \big(F_u^{-1}(h) - t_u(h) \big)^2 \, dh + \int_0^1 \big(F_l^{-1}(h) - t_l(h) \big)^2 \, dh \Big)^{1/2} \tag{2}$$

where $F_u^{-1}(h)$ is the inverse of the upper bound of the CDF, $F_l^{-1}(h)$ the inverse of the lower bound (which both exist because by definition the bounds are non-decreasing), and $t_u(h)$ and $t_l(h)$ are respectively the targets for the upper and lower bound horsetail curves. Note that these targets do not necessarily have to consist of the inverse of valid CDFs; they can be any pair of functions of h. The metric d_{hm} is the L_2 norm of the difference between the horsetail curves and their targets integrated over h. In our horsetail matching formulation, the overall OUU problem becomes finding $\boldsymbol{x}^*$, such that:

$$\boldsymbol{x}^* = \underset{\boldsymbol{x} \in \mathcal{X}}{\operatorname{argmin}} \; d_{hm}(\boldsymbol{x}; t_u, t_l) \tag{3}$$

where the design given by $\boldsymbol{x}^*$ corresponds to the optimal design under uncertainty — its behavior under uncertainty is as close as possible to that specified in the target. Although this formulation might appear to be restrictive since it requires the designer to specify a target, we show in the next section that it is fact flexible enough to recover more traditional robust optimization formulations.

Special Cases

Under exclusively *probabilistic* uncertainties, the metric reduces to:

$$d_{hm}(\boldsymbol{x}) = \Big(2 \int_0^1 \big(F_{cdf}^{-1}(h) - t_{cdf}(h) \big)^2 \, dh \Big)^{1/2} \tag{4}$$

where $F_{cdf}^{-1}(h)$ is the inverse of the CDF and $t_{cdf}(h)$ is its target; this case was explored in detail in [27]. Under exclusively *interval* uncertainties, the metric reduces to:

$$d_{hm}(\boldsymbol{x}) = \Big(\big(q_{min} - t_u \big)^2 + \big(q_{max} - t_l \big)^2 \Big)^{1/2} \tag{5}$$

where q_{min} and q_{max} are the minimum and maximum values of q over all possible values of the uncertain parameters, and t_u and t_l are their respective target values.

B. Flexibility of the Metric

The flexibility of the horsetail matching formulation is a result of the metric in Eq. 2 integrating the L_2 norm over h, since it allows arbitrary functions of h to be used as targets and does not require any overlap of the target with the set of feasible values of q, $\mathcal{Q}$. Other possible metrics that integrate the difference between the CDFs as functions of q (e.g., the Cramer-Von Mises test [28]) would restrict the targets to being inverses of feasible CDFs.

With horsetail matching it is straightforward to provide a target that captures the robust design philosophy of maximizing the likelihood of achieving as good performance as possible. This is achieved by setting both $t_u(h)$ and $t_l(h)$ to be the same constant value of $q = q_{ideal}$ beyond what is attainable. This is the target illustrated in Figure 3, and

is referred to as the "standard target" for horsetail matching. More concretely, a standard target is one that is equal to a constant q_{ideal} such that $q_{ideal} \leq \inf(\mathcal{Q})$ (where $\inf(\mathcal{Q})$ is the infimum of $\mathcal{Q}$: the greatest value that is smaller than any value in $\mathcal{Q}$); if $\mathcal{Q}$ is known then $q_{ideal} = \inf(\mathcal{Q})$ should be used. In many engineering design scenarios this is trivial to identify: zero weight, 100% efficiency, zero cost, zero drag, etc.. Under a standard target, the minimizer of d_{hm} from Eq. 2 will not be stochastically dominated by any other feasible design according to definition II.3, a property we argue is an improvement upon relying on combinations of statistical moments such as in Eq. 1. Also, since the metric is the L_2 norm, it penalizes sections of a CDF further from the target more than it rewards sections closer to the target, giving the metric an intrinsic preference for robustness when a standard target is used.

Additionally, by modifying the shape of a standard target, a target can be set to emphasize the worst values on the horsetail plot and give a *risk averse* optimization [17] (illustrated in Figure 4), or emphasize the best values and give a *risk seeking* optimization (illustrated in Figure 5). The risk averse target can be taken to the extreme such that $t_l(h) \to -\infty$ and only the worst case value is optimized, reducing the formulation back to the "robust regularization" approach [1, 25].

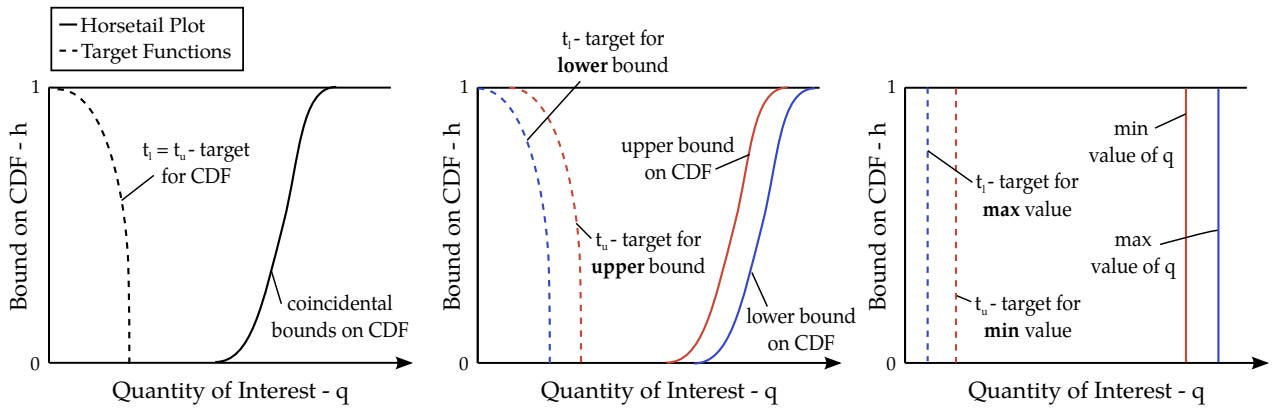

Figure 4: Risk-averse targets (dotted) along with typical horsetail plots (solid) under probabilistic (left), mixed (center), and interval (right) uncertainties. Adapted from [27].

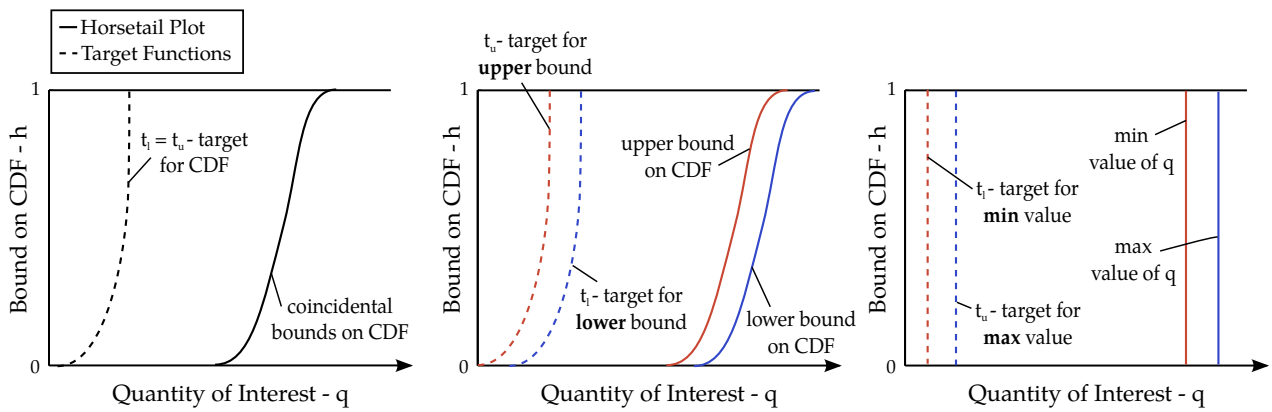

Figure 5: Risk-seeking targets (dotted) along with typical horsetail plots (solid) under probabilistic (left), mixed (center), and interval (right) uncertainties. Adapted from [27].

Alternatively, upper and lower bounds on feasible distributions can be set as the target, or single feasible values, if a designer cares more about the behavior of q around specific values.

C. Numerical Implementation

In order to evaluate d_{hm} in Eq. 2, we need to evaluate integrals that can be expressed in the following:

$$D = \int_0^1 \left(F^{-1}(h) - t(h) \right)^2 dh = \int_{-\infty}^{\infty} \left(q - t(F(q)) \right)^2 F'(q)\, dq \,, \tag{6}$$

where $F(q)$ is either the upper or lower bound on the CDF (one of the two horsetail curves), $F'(q)$ is its derivative with respect to q, $F^{-1}(h)$ is its inverse, and $t(h)$ is its target. In [27], a method of evaluating this integral when $F(q)$ is a single CDF is proposed by making use of kernels to give a differentiable metric, building on the density matching approach in [29]. Here it is extended to mixed uncertainties — when $F(q)$ is a bound on the CDF — by making use of differentiable approximations to the minimum and maximum functions.

Recall that we are interested in a quantity of interest, q, that is a function of probabilistic uncertain parameters, $\boldsymbol{\theta}$, and interval uncertain parameters, $\boldsymbol{\phi}$. Prior to a horsetail matching optimization, N fixed points q_i are specified by the user for the numerical integration which should cover the range of values of q of interest. Additionally, M_θ samples $\boldsymbol{\theta}_j$ are drawn from the distribution of $\boldsymbol{\theta}$, and M_ϕ samples $\boldsymbol{\phi}_m$ are drawn from the hyper-rectangle defined by the intervals of $\boldsymbol{\phi}$. The fixed integration points $\{q_i\colon i = 1, ..., N\}$, the samples $\{\boldsymbol{\theta}_j\colon j = 1, ..., M_\theta\}$, and the samples $\{\boldsymbol{\phi}_m\colon m = 1, ..., M_\phi\}$ are used for every design point $\boldsymbol{x}$ throughout the optimization.

A numerical approximation, $\hat{D}$, to D is computed via three key steps. First, an expression for the CDF of q due to the probabilistic uncertain parameters and its gradient with respect to the design variables are obtained at each value of $\boldsymbol{\phi}_m$ (a single CDF of the ensemble illustrated in Figure 1), resulting in M_ϕ CDFs. Second, an expression for the bounds on the CDFs (the horsetail curves) and the gradients of these bounds are found at the N fixed integration points given by q_i. Finally the difference between these N values of the horsetail curve, h_i, and the values of the corresponding target at each h_i, t_i, are integrated using the trapezium rule to obtain $\hat{D}$. This overall process is outlined in Figure 6 (for the value $\hat{D}$ itself - an equivalent process is used for each component of the gradient), and the algorithms used to achieve these three steps are detailed in Algorithms 1, 2, and 3 below.

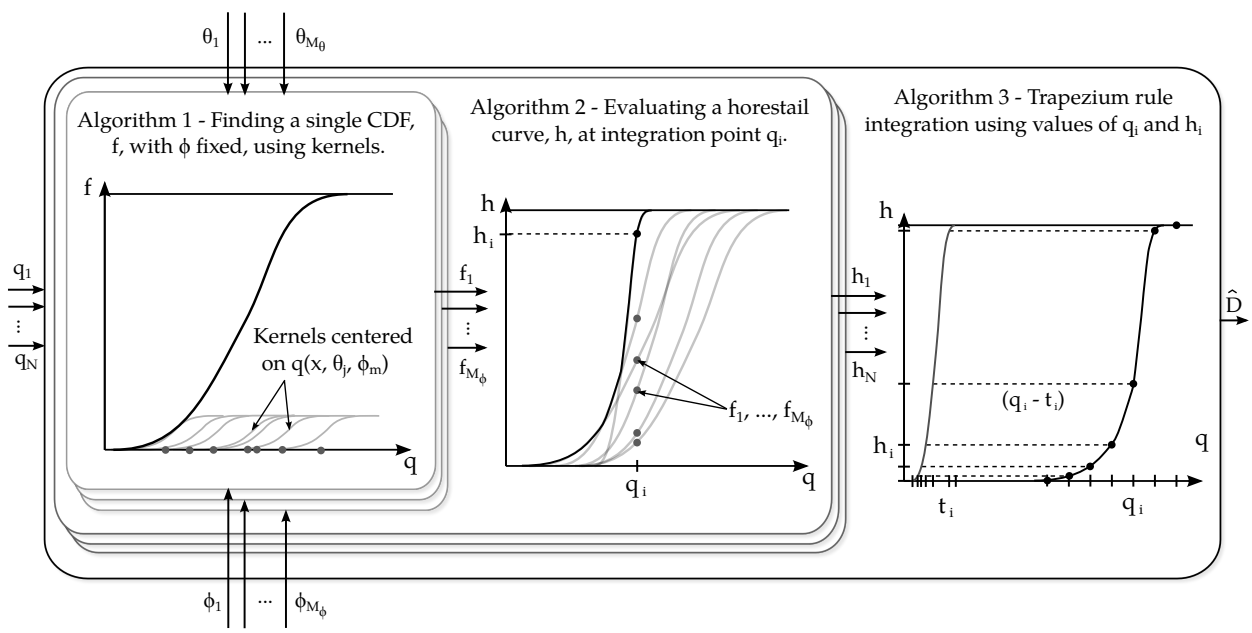

Figure 6: Outline of the numerical implementation of obtaining a numerical approximation, $\hat{D}$, to D in Equation 6 at design $\boldsymbol{x}$, which consists of three key steps that are achieved by Algorithms 1, 2 and 3.

In Algorithm 1, a single CDF at a fixed value of the interval uncertainty $\boldsymbol{\phi}$ is evaluated. Here, K and Φ are kernel functions. We use a Gaussian kernel such that Φ is the error function for a Gaussian and K is its derivative (note that K itself would be used as the kernel function itself in a Kernel density estimation of the PDF [30]):

$$K(r) = \frac{d\Phi(r)}{dr} = \frac{1}{\sqrt{2\pi b^2}} \exp(-\frac{r^2}{2b^2}) \quad \Phi(r) = \frac{1}{2}\left(1 + \mathrm{erf}(\frac{r}{\sqrt{2b^2}})\right) \tag{7}$$

where $r \in Q$ is just the argument of the kernel functions, and b is the bandwidth parameter of the kernel functions, which is fixed throughout the optimization.

In Algorithm 2, values of the horsetail curve at the integration points $\{q_i\colon i = 1, ..., N\}$ are evaluated. Here, S_α gives a differentiable approximation to the maximum or minimum of the M_ϕ values f_m. It is a function that uses exponentials to heavily weight the most extreme values of f_m in a normalized sum of all the values. The sign of the fixed parameter α controls which extremum it approximates and the magnitude of α controls the approximation. As $\alpha \to \infty$, $S_\alpha \to \max(\{f_m\colon m = 1, \ldots, M_\phi\})$ and as $\alpha \to -\infty$, $S_\alpha \to \min(\{f_m\colon m = 1, \ldots, M_\phi\})$.

Algorithm 1 Evaluating a single CDF, f, and its gradient at q with $\boldsymbol{\phi}$ fixed

for $j = 1, \ldots, M_\theta$ **do**
  $q_j \leftarrow$ quantity of interest $q(\boldsymbol{x}, \boldsymbol{\theta}_j, \boldsymbol{\phi})$ from simulation or surrogate model.
  for $k = 1, \ldots, n_x$ **do**
    $\frac{\partial q_j}{\partial x_k} \leftarrow$ gradient of quantity of interest $q(\boldsymbol{x}, \boldsymbol{\theta}_j, \boldsymbol{\phi})$ from simulation or surrogate model.
$f \leftarrow \frac{1}{M_\theta} \sum_{j=1}^{M_\theta} \Phi(q - q_j)$
for $k = 1, \ldots, n_x$ **do**
  $\frac{\partial f}{\partial x_k} \leftarrow \frac{1}{M_\theta} \sum_{j=1}^{M_\theta} K(q - q_j)\,(-1)\,\frac{\partial q_j}{\partial x_k}$
return f, $[\frac{\partial f}{\partial x_1}, \frac{\partial f}{\partial x_k}, \ldots, \frac{\partial f}{\partial x_{n_x}}]$

Algorithm 2 Evaluating a horsetail curve, h, and its gradient at q

for $m = 1, \ldots, M_\phi$ **do**
  $f_m \leftarrow$ value of CDF at q with $\boldsymbol{\phi} = \boldsymbol{\phi}_m$ from Algorithm 1.
  for $k = 1, \ldots, n_x$ **do**
    $\frac{\partial f_m}{\partial x_k} \leftarrow$ gradient of CDF at q with $\boldsymbol{\phi} = \boldsymbol{\phi}_m$ from Algorithm 1.
$h \leftarrow S_\alpha = (\ \sum_{m=1}^{M_\phi} f_m e^{\alpha f_m}\ )/(\ \sum_{m=1}^{M_\phi} e^{\alpha f_m}\ )$
for $k = 1, \ldots, n_x$ **do**
  $\frac{\partial h}{\partial x_k} \leftarrow \sum_{m=1}^{M_\phi} \frac{\partial S_\alpha}{\partial f_m} \frac{\partial f_m}{\partial x_k} = \sum_{m=1}^{M_\phi} \Big(\frac{e^{\alpha f_m}}{\sum_{n=1}^{M_\phi} e^{\alpha f_n}} \Big[1 + \alpha (f_m - S_\alpha) \Big] \frac{\partial f_m}{\partial x_k} \Big)$
return h, $[\frac{\partial h}{\partial x_1}, \frac{\partial h}{\partial x_k}, \ldots, \frac{\partial h}{\partial x_{n_x}}]$

In Algorithm 3, quadrature is employed to find an approximation, $\hat{D}$, of the integral D, as a weighted sum of $(F^{-1}(h) - t(h))^2$ at N values of h:

$$D \simeq \hat{D} = \sum_{i=1}^{N} (\ F^{-1}(h_i) - t(h_i)\ )^2 w_i \tag{8}$$

where h_i are the quadrature points and w_i are the quadrature weights. This is a trapezium rule integration of the integral in Equation 6. It can be considered either as an integration of the first form in Equation 6 where the quadrature points h_i depend on the function $F(q)$, or as an integration of the second form in Equation 6 where the quadrature points q_i are fixed. Note that zeros(N) initializes an array of size N with zeros, and zeros(N, N) an $N \times N$ matrix.

The overall process outlined in Figure 6 consisting of these three algorithms is applied to the upper bound on the CDFs giving $\hat{D}_u \simeq \int_0^1 \ (\ F_u^{-1}(h) - t_u(h)\ )^2\ dh$ and its gradient, as well as the lower bound giving $\hat{D}_l \simeq \int_0^1 \ (\ F_l^{-1}(h) - t_l(h)\ )^2\ dh$ and its gradient. Then finally the numerical approximation to the horsetail matching metric and its gradient are evaluated by $\hat{d}_{hm} = (\hat{D}_u + \hat{D}_l)^{1/2}$ and $\frac{\partial \hat{d}_{hm}}{\partial x_k} = 0.5\,(\frac{\partial \hat{D}_u}{\partial x_k} + \frac{\partial \hat{D}_l}{\partial x_k})\,(\hat{D}_u + \hat{D}_l)^{-1/2}$.

Under purely probabilistic uncertainties, since $h(q)$ is the CDF of $q(\boldsymbol{x}_d, \boldsymbol{\theta})$ and so $\hat{D}_1 = \hat{D}_2$, Algorithm 2 is skipped and the numerical integration in Algorithm 3 is applied directly to the CDF found using Algorithm 1; this is the method used for probabilistic horsetail matching [27]. Under purely interval uncertainties, the horsetail curves become step functions and so kernels are not used to propagate the CDFs and a numerical integration is not performed; instead S_α in Algorithm 2 is used directly to obtain q_{max} (using a large positive value of α) and q_{min} (using a large negative value of α) and their gradients from M_ϕ sampled values of $q_j = q(\boldsymbol{x}_d, \boldsymbol{\phi}_j)$.

Being able to obtain the metric in a differentiable form means that solving a horsetail matching optimization problem using a gradient-based algorithm only requires the ability to obtain values of q and $\frac{\partial q}{\partial x_k}$ at given values of $\boldsymbol{x}$, $\boldsymbol{\theta}$ and $\boldsymbol{\phi}$. If the values of q and $\frac{\partial q}{\partial x_k}$ are readily available, horsetail matching can be implemented as a wrapper treating the available code as a black box. Additionally, in many design problems, $\frac{\partial q}{\partial x_k}$ can be obtained efficiently (e.g., via adjoints in CFD codes [31]), and so being able to propagate this information through to the gradient of d_{hm} is important for keeping the computational cost of the OUU problem low.

The use of Kernels requires the selection of a fixed bandwidth, b, prior to a horsetail matching optimization. This can be done, for example, by using Scott's rule [30] at the initial design, but it is worth noting that a poor choice of

Algorithm 3 Evaluating $\hat{D}$ and its gradient

$\boldsymbol{q} \leftarrow \text{zeros}(N)$
$\boldsymbol{t} \leftarrow \text{zeros}(N)$
$\boldsymbol{W} \leftarrow \text{zeros}(N, N)$
for $i = 1, \ldots, N$ **do**
  $\boldsymbol{q}_i \leftarrow$ fixed integration point q_i
  $h_i \leftarrow$ horsetail curve at q_i from Algorithm 2
  $\boldsymbol{t}_i \leftarrow t(h_i)$ value of t at h_i from the specified target
  $i_1 \leftarrow min(i+1,\ N)$
  $i_2 \leftarrow max(i-1,\ 1)$
  $\boldsymbol{W}_{i,i} \leftarrow 0.5(\ h_{i_1} - h_{i_2}\ )$
$\hat{D} \leftarrow (\boldsymbol{q} - \boldsymbol{t})^T \boldsymbol{W} (\boldsymbol{q} - \boldsymbol{t})$
for $k = 1, \ldots, n_x$ **do**
  $\frac{\partial \boldsymbol{t}}{\partial x_k} \leftarrow \text{zeros}(N)$
  $\frac{\partial \boldsymbol{W}}{\partial x_k} \leftarrow \text{zeros}(N, N)$
  for $i = 1, \ldots, N$ **do**
    $\frac{\partial h_i}{\partial x_k} \leftarrow$ gradient of the horsetail curve at q_i from Algorithm 2
    $t' \leftarrow$ derivative of t with respect to the argument, $\frac{\partial t(h)}{\partial h}$, at h_i from the specified target
    $(\frac{\partial \boldsymbol{t}}{\partial x_k})_i \leftarrow t' \frac{\partial h_i}{\partial x_k}$
    $i_1 \leftarrow min(i+1,\ N)$
    $i_2 \leftarrow max(i-1,\ 1)$
    $(\frac{\partial \boldsymbol{W}}{\partial x_k})_{i,i} \leftarrow 0.5(\ \frac{\partial h_{i_1}}{\partial x_k} - \frac{\partial h_{i_2}}{\partial x_k}\ )$
  $\frac{\partial \hat{D}}{\partial x_k} \leftarrow 2(\boldsymbol{q} - \boldsymbol{t})^T \boldsymbol{W} (-\frac{\partial \boldsymbol{t}}{\partial x_k})\ +\ (\boldsymbol{q} - \boldsymbol{t})^T \frac{\partial \boldsymbol{W}}{\partial x_k} (\boldsymbol{q} - \boldsymbol{t})$
return $\hat{D}$, $[\frac{\partial \hat{D}}{\partial x_1}, \frac{\partial \hat{D}}{\partial x_k}, \ldots, \frac{\partial \hat{D}}{\partial x_{n_x}}]$

bandwidth can lead to a highly non-smooth gradient (if b is too small) or can give smooth but erroneous values of d_{hm} and its gradient (if b is too large).

Surrogate Modeling for Computational Efficiency

A high number of samples (both of $\boldsymbol{\phi}$ and $\boldsymbol{\theta}$) are required to accurately propagate this metric and the gradient within an optimization, which may be infeasible to do via direct sampling if an expensive simulation is used to find q and $\frac{\partial q}{\partial x_k}$. Therefore surrogate models can first be fitted to q as well as to $\frac{\partial q}{\partial x_k}, k = 1, \ldots, n_x$ as a function of $\boldsymbol{\theta}$ and $\boldsymbol{\phi}$ for each design $\boldsymbol{x}_d$. Surrogate models have been shown to be useful for propagating uncertainties in various applications of design under uncertainty [19, 32–34]; in particular propagating mixed uncertainties by sampling surrogate models has been demonstrated to be effective [7, 10]. These surrogate models can then be sampled as many times as required at small computational cost (assuming the computational expense of the simulation vastly outweighs evaluating the surrogate model). This also means that it is no more expensive to propagate d_{hm} under mixed uncertainties than probabilistic or interval uncertainties since fitting a surrogate model for q as a function of the uncertain parameters is the same cost regardless of how it is sampled afterwards.

IV. Experiments on an Algebraic Test Problem

In order to assess the effectiveness of the numerical implementation of the approach, here horsetail matching under mixed uncertainties is tested on an algebraic test problem. The test problem in Eq. 9 is used (an algebraic problem allows many optimizations to be run at low computational cost), where q is a function of two design variables x_1 and x_2 that are each bounded by $[-5, 5]$, one probabilistic uncertain parameter, θ, which is uniformly distributed over the range $[-1, 1]$, and one interval uncertain parameter, ϕ, which is contained in the interval $[-1, 1]$.

$$
\begin{aligned}
y &= x_1/2 \\
z &= x_2/2 + 12 \\
q &= 0.25((y^2 + z^2)/40 + 5y\theta\phi - z\phi^2) + 0.2(z\phi^3) + 10
\end{aligned}
\tag{9}
$$

Figure 7 shows horsetail plots for this test problem at the design point $\boldsymbol{x} = (4, 2)$. The method in Section III:C is used to propagate the CDF from $M_\theta = 100$ samples of θ for each value of ϕ (plotted in grey) and then find the envelope of the $M_\phi = 30$ CDFs at $N = 1000$ integration points q_i evenly spaced between $q = -5$ and $q = 30$. To determine an appropriate value of α to use in S_α, Algorithm 2 is performed using different values of α.

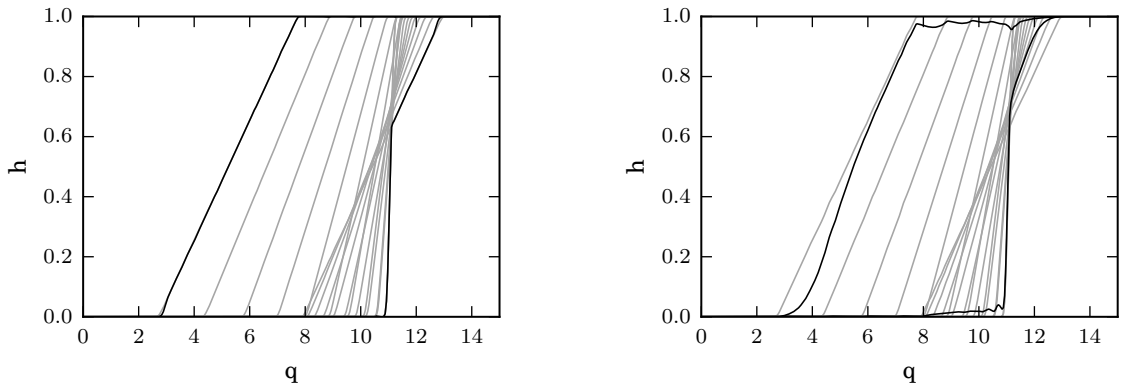

(a) Mixed, $\alpha = 100$

(b) Mixed, $\alpha = 10$

Figure 7: Propagated horsetail plots of the test problem using $\alpha = 100$ and $\alpha = 10$.

It can be seen that the method for $\alpha = 100$ obtains the envelope of the CDFs to visible accuracy, whereas $\alpha = 10$ gives a poor approximation to the envelope. Therefore $\alpha = 100$ is used for the horsetail matching optimizations in this section. Furthermore, for this test problem, the mixed case for $\alpha = 0$ is equivalent to the purely probabilistic case where ϕ is uniformly distributed, since the samples of ϕ are drawn uniformly from the interval $[-1, 1]$. These two cases are compared in Figure 8.

Optimization Tests

A gradient-based optimizer (SLSQP, implemented using the NLopt toolbox [35]) is run on the test problem from 50 random starting points in design space, where the standard target at $q = 0$ is used. The propagated gradient is found from the sensitivity of q to design variables, $\frac{\partial q}{\partial x_k}$, which is obtained from the analytic derivative of Eq. 9 at the sample points. Convergence histories are plotted in Figure 9. The difference between the horsetail matching (HM) metric and the best value obtained from all 50 optimizations is plotted, where a difference of 10^{-3} is considered converged. It can be observed that the optimizer solves the horsetail matching problem from all 50 starting points, indicating the effectiveness of the numerical implementation outlined in Section III:C.

V. Application to Aero-Structural Design Problem

In this section, horsetail matching is applied to a physical aero-structural design test problem subject to mixed uncertainties. The design problem involves determining the geometry of a wing in order to minimize the fuel burn for a given mission subject to lift and failure constraints. It uses a low fidelity coupled aero-structural analysis code[a] that utilizes a vortex lattice method aerodynamics model expanded from a modern lifting line theory, and a linear 6-DOF-per-element spatial beam structural model. The code is built on the OpenMDAO architecture [36] to efficiently analyze the coupled simulation and its gradient. An illustration of a wing analyzed using this code is given in Figure 10 (note that it is just a single wing that is analyzed).

For the design problem considered here, the wing mesh is built from a total of 11 evenly spaced spanwise points and 4 chordwise points. The wing design is parametrized by controlling the span, taper ratio, sweep, and angle attack

[a] https://github.com/hwangjt/OpenAeroStruct

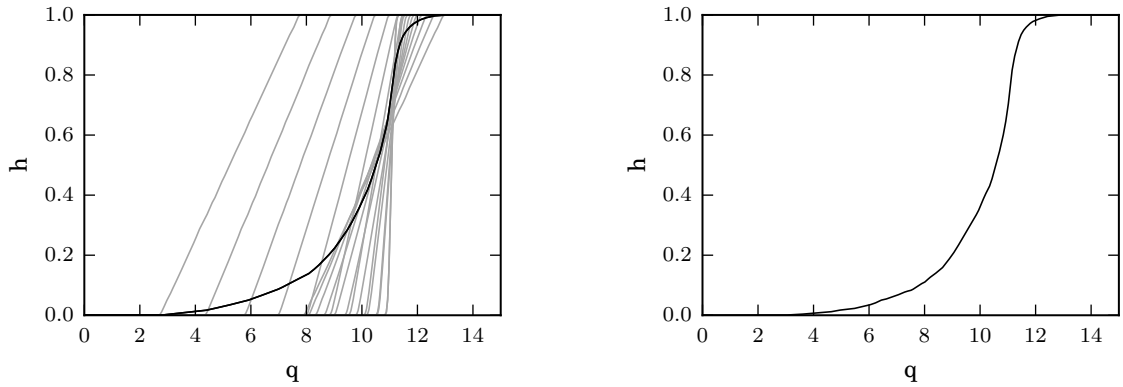

(a) Mixed, $\alpha = 0$

(b) Probabilistic

Figure 8: Propagated horsetail plot of the test problem using $\alpha = 0$ and propagated probabilistic CDF

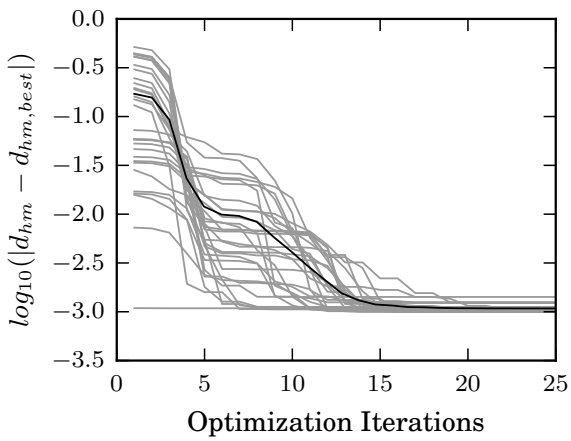

Figure 9: Horsetail matching optimization convergence histories under mixed uncertainties using the propagated gradient on the algebraic test problem.

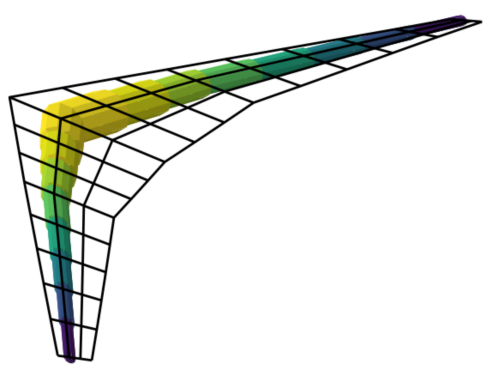

Figure 10: Illustration of the OpenAeroStruct flying wing model[a].

of the wing, along with the thickness and twist at three spanwise control points for half of the span (the wing is symmetric), giving a total of $n_x = 10$ design variables. The overall design space, $\mathcal{X}$, for this problem is given in Table

1.

Notation	Design Variable	Lower Bound (x_k^L)	Upper Bound (x_k^U)	Units
x_1	Span	40	70	m
x_2	Taper Ratio	0	0.9	-
x_3	Sweep	10	40	deg
x_4	Nominal Angle of Attack	0	20	deg
x_5	Twist at Loc. 1	−5	20	deg
x_6	Twist at Loc. 2	−5	20	deg
x_7	Twist at Loc. 3	−5	20	deg
x_8	Thickness at Loc. 1	0.1	0.3	m
x_9	Thickness at Loc. 2	0.1	0.3	m
x_{10}	Thickness at Loc. 3	0.1	0.3	m

Table 1: Design space for the flying wing design problem.

We consider two probabilistic uncertain parameters, θ_1 and θ_2, and one interval uncertain parameter, ϕ. The probabilistic uncertain parameters represent uncertainty in the operating conditions of the flying wing: the Mach number is uniformly distributed from 0.65 to 0.75, and the actual angle of attack is distributed uniformly over a 4 degree range centered on the nominal angle of attack which is denoted by γ_{nom} and given by design variable x_4. The interval uncertain parameter represents uncertainty in the material properties: the failure stress is in the interval $[15, 25]$ MPa. The different representations for the uncertain parameters are chosen to illustrate how our formulation handles mixed uncertainties, these representations are detailed in Table 2.

Notation	Uncertain Parameter	Type	Range	Units
θ_1	Mach Number	Uniform Distribution	$[0.65, 0.75]$	m
θ_2	Actual Angle of Attack	Uniform Distribution	$[\gamma_{nom} - 2, \gamma_{nom} + 2]$	deg
ϕ	Failure Stress	Interval	$[15, 25]$	MPa

Table 2: Uncertain parameters for the flying wing design problem.

The objective is to minimize the fuel burn for a given mission subject to the lift constraint given by equation 10 and the failure constraint given by equation 11 being satisfied. The lift constraint ensures the lift generated by the wing is sufficient to balance the weight:

$$g_1 := \frac{W_0 + W_{structural} + W_{fuel} - L}{W_0} \leq 0, \tag{10}$$

where W_0 is the baseline weight of the wing, $W_{structural}$ is the structural weight of the wing, W_{fuel} is the weight of fuel burnt over the range, and L is the lift. The failure constraint is a Kreisselmeier-Steinhauser (KS) combination of the von Mises stresses in each element to obtain a single non-linear constraint function [37]:

$$\begin{aligned} f_{max} &= \max\left(\frac{\sigma_{vm,i}}{\sigma_{fail}}\right), \\ g_2 := f_{max} &+ \frac{1}{\rho}\log\sum_i \rho\left(\frac{\sigma_{vm,i}}{\sigma_{fail}} - 1 - f_{max}\right) \leq 0, \end{aligned} \tag{11}$$

where ρ is the KS tolerance parameter (set to 10), $\sigma_{vm,i}$ is the von Mises stress for each element, and σ_{fail} is the failure stress of the material (set to 20 GPa).

These constraints are taken into account in the optimizations using squared penalty functions so that, denoting the fuel burn as m_{fuel} (in units of $kg \times 10^6$), the total quantity of interest for this design problem becomes:

$$q(\boldsymbol{x}, \theta_1, \theta_2, \phi) = m_{fuel} + 3(\max(g_1, 0))^2 + 3(\max(g_2, 0))^2 \tag{12}$$

The remaining parameters used to set up the OpenAeroStruct analysis are given in Table 3.

OpenAeroStruct Notation	Parameter	Value	Units
Alt	Altitude	30000	feet
E	Elastic Modulus	200×10^9	Pa
G	Shear Modulus	30×10^9	Pa
mrho	Material Density	3×10^3	kg/m^3
W0	Base Weight	1.00×10^5	kg
CL0	Base Lift Coefficient	0.25	-
CD0	Base Drag Coefficient	0.015	-
SFC	Specific Fuel Consumption	17×10^6	$1/s$
chord	Chord at Wing Root	12	m
R	Range	10×10^6	m

Table 3: Parameters used in the OpenAeroStruct analysis of the flying wing.

Optimization Results

We compare designs resulting from different types of optimizations on the design problem to compare horsetail matching to alternative approaches. For all these optimizations, the gradient-based SLSQP algorithm is used, implemented with NLopt [35], and is run for 20 iterations (representing a fixed computational budget) after which the best design is taken as the optimum. First we run a deterministic optimization with the uncertain parameters at their nominal values, and then we run horsetail matching using a standard target, a risk averse target, and a single feasible value target. The optimizations are all run from an initial design given by each design variable x_k taking the value at the midpoint of its bounds.

The differences between the designs are small enough that plotting the wing mesh in each case is not illustrative, instead we give the horsetail plots for each design in Figure 11, and the values of the design variables for the optimum design in each case are given in Table 4.

The deterministic optimization minimizes the nominal value of the quantity of interest (with $\theta_1 = \theta_2 = \phi = 0$):

$$\begin{aligned} \underset{\boldsymbol{x}}{\text{minimize}} \;\; & q(\boldsymbol{x}, \theta_1 = 0, \theta_2 = 0, \phi = 0) \\ \text{s.t. } & x_k^L < x_k < x_k^U \;\; k = 1, \ldots, 10 \end{aligned} \tag{13}$$

The horsetail matching optimizations minimize the horsetail matching metric d_{hm} from Equation 2, where the value and the gradient are evaluated using the approach outline in Section III:C, given the specified target functions $t_u(h)$ and $t_l(h)$:

$$\begin{aligned} \underset{\boldsymbol{x}}{\text{minimize}} \;\; & d_{hm}(q(\boldsymbol{x}, \theta_1, \theta_2, \phi);\; t_u,\; t_l) \\ \text{s.t. } & x_k^L < x_k < x_k^U \;\; k = 1, \ldots, 10. \end{aligned} \tag{14}$$

For this design problem, a three dimensional, third order polynomial surrogate is fitted to the quantity of interest, q, and each component of its gradient, $\frac{\partial q}{\partial x_k}$, as a function of the uncertain parameters, θ_1, θ_2 and ϕ, at each design point. This corresponds to $4^3 = 64$ calls of the OpenAeroStruct analysis code at each iteration, giving a total computational budget of $64 \times 20 = 1280$ calls for each horsetail matching optimization. We again use $\alpha = 100$.

The targets for the horsetail matching optimizations are assigned as follows: a standard target is used by setting $t_l(h) = t_u(h) = 0$ (as we know q can never reach zero). The risk averse target is obtained by skewing the top of the target for the lower bound of the CDF (the right-most horsetail curve) to a value of -10 from the base standard target at $q = 0$, the target at a specific value of $q = 1.3$ is used to minimize variation around this value.

We can see on Figure 11 that since the deterministic optimization did not take into account the uncertainties, the bounds on the CDF both have tails at large values of the quantity of interest (which represents fuel burn plus penalties for constraint violation), indicating a high likelihood that this design will give degraded performance in reality. In contrast, the horsetail plot for the horsetail matching optimum design under the standard target gives bounds on the CDFs whose tails do not reach as large values of q, indicating improved robustness under mixed uncertainties, whilst only taking a small penalty to the best possible value.

We can also see that the risk averse design is similar to the standard horsetail matching optimum design, but it has a slightly better worse-case performance (the highest value of q reached by the lower bound on the CDF). Finally, the

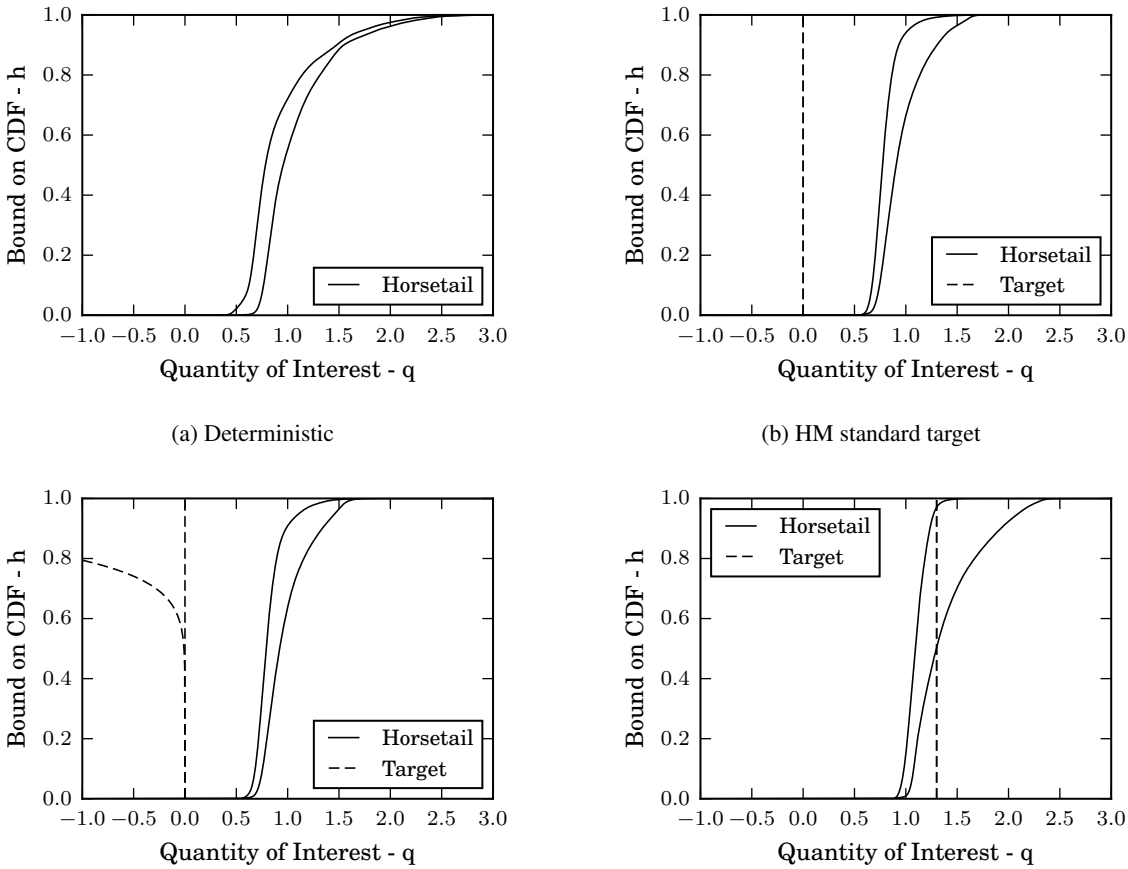

(a) Deterministic

(b) HM standard target

(c) HM risk averse target

(d) HM feasible value target

Figure 11: Horsetail plots for the optimum designs

optimum under a single value target gives a horsetail plot that is close to the target value, and we can see from Table 1 that this design is noticeably different to the other designs.

These cases clearly demonstrate the flexibility of the horsetail matching formulation, as designs with horsetail plots with different properties, representing optimization under different design scenarios, were obtained simply by changing the target used in the optimization.

Comparsion to the Weighted Sum Approach

Finally we compare horsetail matching to the method commonly suggested in the literature for optimization under mixed uncertainties: using a weighted sum of midpoints and ranges of intervals of statistical moments of the possible CDFs that the horsetail plot bounds [9–12]. The interval of means of possible CDFs is given by $[\mu_{min}, \mu_{max}]$, and the interval of standard deviations is given by $[\sigma_{min}, \sigma_{max}]$ The following weighted sum of three objectives is optimized:

$$f_{obj} = w_1\bar{\mu} + w_2\bar{\sigma} + w_3\delta\mu \tag{15}$$

where $\bar{\mu}$ is the average of μ_{min} and μ_{max}, $\bar{\sigma}$ is the average of σ_{min} and σ_{max}, and $\delta\mu$ is the difference between μ_{min} and μ_{max}. To propagate these three objectives, the method outlined in Ref. 10 is used, where polynomial chaos expansions of q as a function of the uncertain parameters are used to find expressions for μ and σ as functions of the interval uncertain parameters $\boldsymbol{\phi}$, which are then optimized over $\boldsymbol{\phi}$ to obtain μ_{min}, μ_{max}, σ_{min}, and σ_{max} for use in Eq. 15. Since this method uses a surrogate model at each design point, each optimization iteration has the same computational cost as the horsetail matching implementation; third order polynomials in each dimension are used in both cases.

The weights are selected using the method suggested in Refs. 12 and 10: by looking at the relative magnitudes of the three objectives at the deterministic optimum design and selecting weights so that they all have the same

contribution to f_{obj} for this design. For this design problem, at the deterministic optimum the three objectives are $\bar{\mu} = 1.00$, $\bar{\sigma} = 0.392$, and $\delta\mu = 0.0745$, so the weights are selected as $w_1 = 1.00$, $w_2 = 2.55$, and $w_3 = 13.43$. Thus the following problem is optimized:

$$\begin{aligned} \underset{x}{\text{minimize}} \;\; & \bar{\mu} + 2.56\,\bar{\sigma} + 13.43\,\delta\mu \\ \text{s.t. } & x_k^L < x_k < x_k^U \;\; k = 1, \ldots, 10 \end{aligned} \tag{16}$$

The results of this weighted sum optimization are given in Figure 12, where the horsetail plot (Weighted Sum) is compared to the plot for the horsetail matching optimum using the standard target (labeled Standard HM).

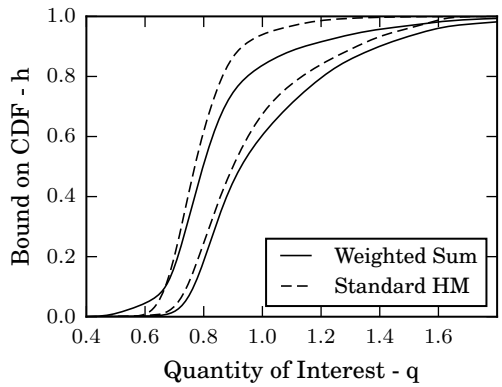

Figure 12: Horsetail plot for the final design of a weighted sum optimization, along with the horsetail plot from the horsetail matching optimum design under the standard target. (Note the scale is different to Figure 11).

It can be observed from Figure 12 that the optimum design using these weights is close to being stochastically dominated by the horsetail matching optimum design under the standard target: the lower bound on the CDF lies entirely to the right of the lower bound for the standard HM optimum and the upper bound is only better for $h < 0.1$. This highlights the limitations that were discussed in Section I of using a weighted sum of combinations of statistical moments as the objective to be minimized in an optimization as in Equation 16.

Table 4 gives the design variables for the optimum designs from the deterministic optimization, the horsetail matching optimizations under the standard target ($t_l(h) = t_u(h) = 0$), the risk-averse target, and the target at a specific feasible value ($t_l(h) = t_u(h) = 1.3$) as well as the weighted sum optimization.

	Deterministic	Standard	Risk Averse	Specific Value	Weighted Sum
Span	55	53.63	54.14	53.5	52.6
Taper Ratio	0.1	0.118	0.119	0.305	0.118
Sweep	10	10	10	10.9	10.0
Nominal Angle of Attack	9.5	10.2	10.19	10.4	10.2
Twist at Loc. 1	9.20	9.14	8.84	10.0	9.13
Twist at Loc. 2	2.0	2.47	2.72	3.56	2.47
Twist at Loc. 3	-1.0	0.14	-0.21	0.76	0.15
Thickness at Loc. 1	0.1	0.1	0.1	0.13	0.1
Thickness at Loc. 2	0.1	0.1	0.1	0.13	0.1
Thickness at Loc. 3	0.1	0.1	0.1	0.12	0.1

Table 4: Design parameters for the optimum designs from the different optimization cases

VI. Application To Transonic 3D Wing Design

To demonstrate how the proposed approach and implementation makes use of adjoint sensitivity information in a practical CFD-based design problem, in this section horsetail matching is applied to the shape optimization of a 3D wing in transonic flow conditions, subject to uncertainties in Mach number and angle of attack.

A. Problem Setup

The quantity of interest for the wing is taken as lift-to-drag ratio, measuring performance at cruise, and it is subject to a uniformly distributed Mach number between 0.80 and 0.86 and an interval uncertain parameter on the angle of attack between 2.5° to 3.5°. We note a lift-constrained drag optimization would be more representative of realistic wing design than a lift-to-drag ratio optimization, but since the purpose of this section is to investigate the effectiveness of horsetail matching in manipulating the behavior of a wing under uncertainty using adjoint sensitivity information, this does not impact the conclusions of this section. We use lift-to-drag ratio as the objective so that this study can be performed at reasonable computational cost.

The lift-to-drag ratio is computed using the openly available SU2 CFD package to solve the compressible RANS equations; this solver has been validated on a number of test cases including the ONERAM6 wing used as the baseline design for this study [38,39]. The design space is parameterized using a free form deformation (FFD) box that encloses the wing and consists of six chord-wise (x-direction), six span-wise (y-direction) and two vertical (z-direction) control points. The control points can move in the vertical direction (except the control points in the two y=constant planes closest to the symmetry boundary condition, which are fixed) giving a total of 48 design variables; these points are used to deform a baseline mesh on the ONERAM6 wing (which is provided with SU2 and is made up of a total of 545,438 elements and 96,252 points) using the mesh deformation capability within SU2. Additionally, the sensitivity of lift-to-drag ratio to the design variables is evaluated by solving the adjoint equations for the flow, once for lift and once for drag, using the adjoint solver capabilities within SU2.

A view of this mesh on the wing and symmetric boundary condition plane at y=0 is shown on Figure 13, along with the outline of the FFD box in white.

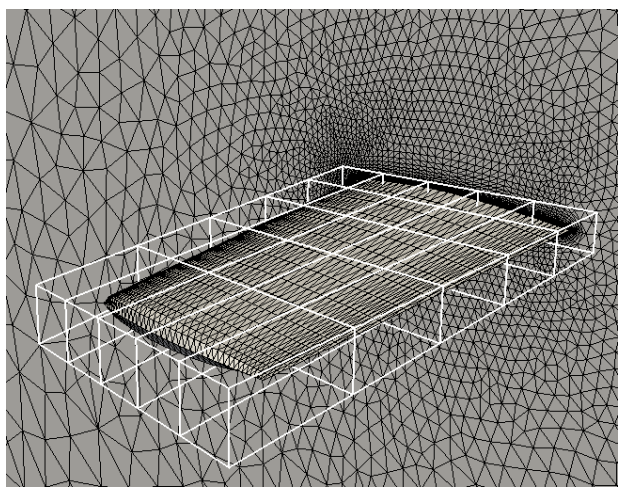

Figure 13: FFD box and mesh

A top-down plan view of the baseline wing C_p contours in nominal flow conditions ($M = 0.83$, $AoA = 3.0°$) are given in Figure 14.

To propagate the uncertainties for a given design, a third order, two dimensional polynomial response surface is fitted to a tensor grid of evenly spaced points over the uncertainty domain, to give a surrogate model for both the quantity of interest itself and its sensitivity to each of the design variables. This requires 16 forward and 32 adjoint CFD solves per design iteration. These surrogate models are then sampled 2000 times each at 25 values of the interval uncertain parameter, totaling 100,000 samples, to propagate the horsetail plot and its gradient as described in Section III:C. This is done on the baseline ONERAM6 design and the resulting horsetail plot is given in Figure 15.

We can observe that at nominal conditions, the baseline ONERAM6 wing demonstrates a typical planform lambda shock pattern, and the horsetail plot gives a significant drop off in performance from the nominal value of $L/D = 14.1$ on both the upper and lower CDF bounds, whilst the best possible case over the uncertain parameters is only $\simeq 14.7$. Therefore we expect significant improvement of the lift-to-drag ratio under uncertainty to be possible using horsetail matching.

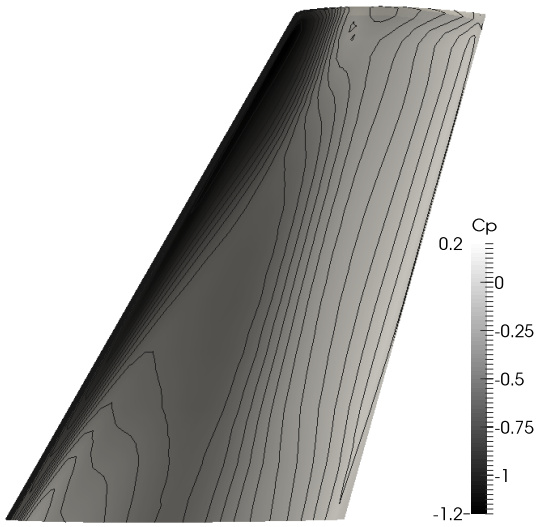

Figure 14: Upper surface pressure contours for the baseline ONERAM6 wing in nominal flow conditions; lift-to-drag ratio = 14.1.

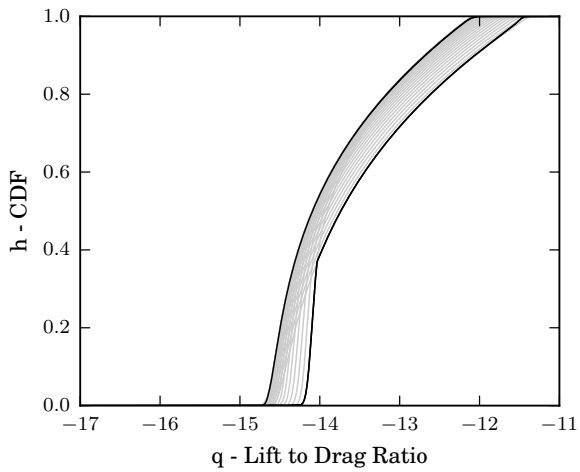

Figure 15: Horsetail plot of lift-to-drag ratio for the baseline ONERAM6 wing. Grey lines indicate the evaluated possible CDFs of which the horsetail plot gives the envelope.

B. Optimization Results

The optimizations in this section are performed using the SLSQP implementation in the NLopt toolbox [35] (as in Section IV). We run two horsetail matching optimizations, both using $\alpha = 100$, firstly under a standard target with $q_{ideal} = 20$:

$$\begin{aligned} \underset{\boldsymbol{x}}{\text{minimize}} \;\; & d_{hm}(q(\boldsymbol{x}, M \sim \mathcal{U}(0.80, 0.86), AoA \in [2.5^\circ, 3.5^\circ];\; t_u(h) = -20,\; t_l(h) = -20) \\ \text{s.t.} \;\; & -0.05 < x_k < 0.05 \;\; k = 1, \ldots, 48. \end{aligned} \tag{17}$$

Secondly under a risk averse target for both bounds on the CDF (where the value of $t_l(1)$ and $t_u(1)$ is set to -60), in order to emphasize improving the robustness over the best possible lift-to-drag ratios:

$$\begin{aligned} \underset{\boldsymbol{x}}{\text{minimize}} \;\; & d_{hm}(q(\boldsymbol{x}, M \sim \mathcal{U}(0.80, 0.86), AoA \in [2.5^\circ, 3.5^\circ];\; t_u(h) = -20 - 40(h)^5),\; t_l(h) = -20 - 40(h)^5) \\ \text{s.t.} \;\; & -0.05 < x_k < 0.05 \;\; k = 1, \ldots, 48. \end{aligned} \tag{18}$$

The convergence of the SLSQP algorithm for these optimizations, shown as iteration against relative difference between the objective and the best objective, is given in Figure 16. In order to fairly compare the designs resulting from each optimization, we analyze them at a given operating point, taken as that of the baseline wing with the uncertain parameters at their nominal values, which is $M = 0.83$ and $C_L = 0.260$; the angle of attack is adjusted to give this lift coefficient. The force coefficients of the designs at this operating point are given in Table 5. The horsetail plot of $-1\times$ lift-to-drag ratio due to the uncertainties for the designs are given in Figure 18.

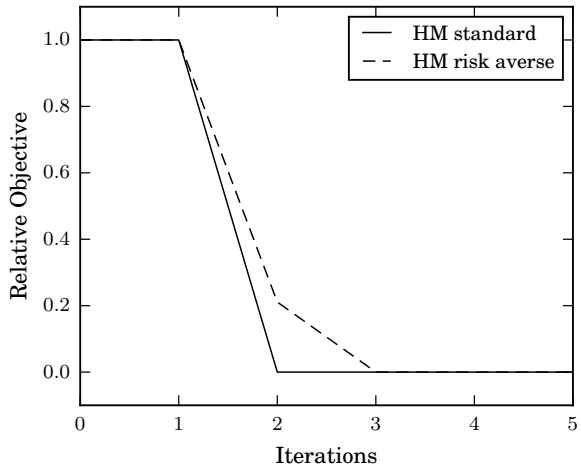

Figure 16: Relative convergence of the two wing optimizations.

The pressure contours of the design resulting from the optimization under a standard target at the given operating point is given in Figure 17. By examining the flow solutions (as well as the deformed FFD points), we can see that this optimization has improved the design by lowering the FFD points at the leading edge of the wing and raising them towards the trailing edge, effectively decreasing the angle of incidence of the wing towards the tip while increasing the camber and decreasing the twist at the tip. From the forces at the given operating point in Table 5, we can see that for the same C_L the drag has reduced relative to the baseline. This is due to a reduction in pressure drag (the friction drag increases), and we can see that the strong shock at the tip of the baseline design has been eliminated, removing the lambda shock structure.

	ONERAM6	Standard	Risk Averse
M	0.83	0.83	0.83
C_L	0.260	0.260	0.260
AoA	3.0°	3.16°	3.03°
$C_{D,\,total}$	0.0184	0.0170	0.0170
$C_{D,\,friction}$	0.0046 (25%)	0.00475 (27%)	0.00474 (27%)
$C_{D,\,pressure}$	0.0138 (75%)	0.0123 (73%)	0.0123 (73%)
L/D	14.1	15.3	15.3

Table 5: Force coefficients at the given operating point ($M = 0.83, C_L = 0.260$) for the baseline wing and the two optimized designs

The design resulting from the optimization under a risk averse target is a similar shape to and follows similar pressure contours at nominal conditions to the standard target case, so we just give the force coefficients in Table 5 and the horsetail plot of this design in Figure 18.

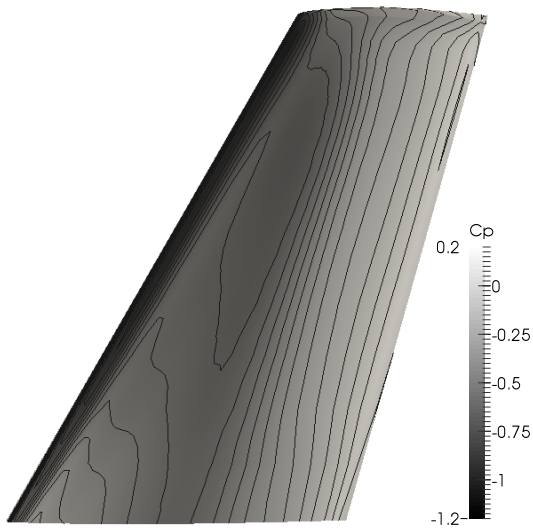

Figure 17: Upper surface pressure contours for the horsetail matching optimum under a standard target $t(h) = -20$ at $(M = 0.83, C_L = 0.260)$.

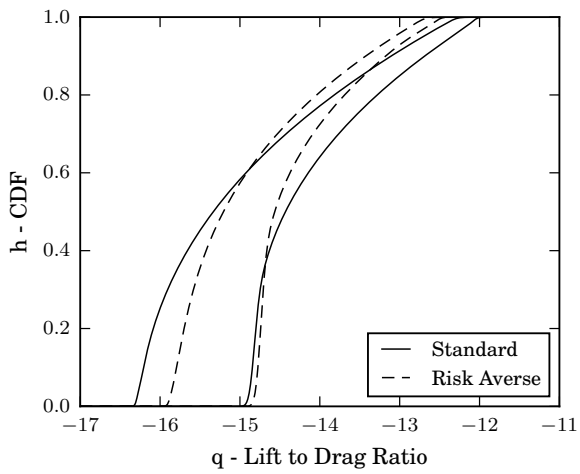

Figure 18: Comparison of horsetail plots of $-1\times$ lift-to-drag ratio of the designs found from the two optimizations

From observing the horsetail plot for the design from the optimization using a standard target in Figure 18, we can see that its behavior under uncertainty is significantly more favorable than the baseline design. The horsetail plot consists of bounds on the CDF that give better lift-to-drag ratios for all values of h, indicating that this design stochastically dominates the baseline design under mixed uncertainties according to definition II.3.

Additionally, we can see that even though the design obtained using a risk averse target gives very similar performance at nominal conditions to the standard case, it gives different behavior under uncertainty. The risk averse design has traded off the best possible performance over the horsetail plot for additional robustness: the tails of the horsetail plot for the risk averse design give better performance than the standard design, and the bounds on the CDF are closer together.

The similarity of the performance of the designs in Table 5 highlights the fact that only considering in the design nominal conditions does not necessarily produce desirable behavior under uncertainty. Additionally Figure 18 clearly demonstrates the influence of the target on the optimization and the ability of horsetail matching to effectively manipulate the behavior under mixed uncertainties of the wing, and how by making use of sensitivity information from

adjoint CFD solves it is able to do so efficiently.

VII. Conclusion

Horsetail matching is extended to optimization under probabilistic, interval, and mixed uncertainties, and a numerical implementation that delivers a single, differentiable metric for optimization is developed. The approach is applied to the design of a wing analyzed using a low-fidelity, coupled aero-structural analysis code; on this physical problem the flexibility of horsetail matching is demonstrated by using different targets to optimize for different design scenarios at low computational cost. It is also compared to the weighted sum of combinations of statistical moments approach, and on this problem it gives preferable designs at similar computational cost. The approach is also applied to the shape optimization of a 3D wing under uncertainties in Mach number and angle of attack, where by making use of sensitivity information from adjoint CFD solves it is shown to efficiently improve the behavior under uncertainty of the wing. For this problem a risk averse target produced a more robust wing design than a standard target.

Planned future work into horsetail matching primarily involves investigating and improving the formulation when a large number of uncertain parameters are involved in the problem, since the effectiveness of using surrogate models to propagate the uncertainty deteriorates rapidly as the dimensionality of the uncertainty space increases; this is considered a limitation of the implementation proposed in this paper. A formal analysis of the approximation error of the proposed numerical implementation is also an important issue to address. Additionally, at increased computational cost, demonstrating horsetail matching in a lift-constrained drag minimization wing design setting would be a useful avenue of future work.

Acknowledgments

This work is funded by the Engineering and Physical Sciences Research Council (EPSRC) UK, grant number EP/L504920/1. The third author acknowledges support of the Air Force Office of Scientific Research (AFOSR) MURI on managing multiple information sources of multi-physics systems, Program Manager Jean-Luc Cambier, Award Number FA9550-15-1-0038. The research data supporting this publication, which consists of the software used to perform the optimizations is available through the horsetail matching python module which is available at *http://www-edc.eng.cam.ac.uk/aerotools/horsetailmatching/*, and is archived at *https://doi.org/10.17863/CAM.12577*.

References

[1] Beyer, H. G. and Sendhoff, B., "Robust Optimization - A Comprehensive Survey," *Computer Methods in Applied Mechanics and Engineering*, Vol. 196, No. 33-34, 2007, pp. 3190–3218.

[2] Kennedy, M. C. and O'Hagan, A., "Bayesian Calibration of Computer Models," *Journal of the Royal Statistical Society. Series B (Statistical Methodology)*, Vol. 63, No. 3, 2001, pp. 425–464.

[3] Du, X. and Chen, W., "Methodology for Managing the Effect of Uncertainty in Simulation-Based Design," *AIAA Journal*, Vol. 38, No. 8, 2000.

[4] Keane, A. J. and Nair, P. B., *Computational Approaches for Aerospace Design: The Pursuit of Excellence*, Wiley, New York, 2005.

[5] Helton, J. C., Johnson, J. D., and Oberkampf, W. L., "An Exploration of Alternative Approaches to the Representation of Uncertainty in Model Predictions," *Reliability Engineering and System Safety*, Vol. 85, No. 1-3, 2004, pp. 39–71.

[6] Eldred, M. S., Swiler, L. P., and Tang, G., "Mixed Aleatory-Epistemic Uncertainty Quantification With Stochastic Expansions and Optimization-Based Interval Estimation," *Reliability Engineering and System Safety*, Vol. 96, No. 9, 2011, pp. 1092–1113.

[7] Hosder, S. and Bettis, B., "Uncertainty and Sensitivity Analysis for Reentry Flows with Inherent and Model-Form Uncertainties," *Journal of Spacecraft and Rockets*, Vol. 49, No. 2, 2012, pp. 193–206.

[8] West, T. K., Hosder, S., and Johnston, C. O., "Multistep Uncertainty Quantification Approach Applied to Hypersonic Reentry Flows," *Journal of Spacecraft and Rockets*, Vol. 51, No. 1, 2014, pp. 296–310.

[9] Rumpfkeil, M. P., "Robust Design Under Mixed Aleatory / Epistemic Uncertainties Using Gradients and Surrogates," *Journal of Uncertainty Analysis and Applications*, 2013.

[10] Zhang, Y. and Hosder, S., "Robust Design Optimization Under Mixed Uncertainties With Stochastic Expansions," *Journal of Mechanical Design*, Vol. 135, 2013.

[11] Shah, H., Hosder, S., Koziel, S., Tesfahunegn, Y., and Leifsson, L., "Multi-fidelity Robust Aerodynamic Design Optimization Under Mixed Uncertainty," *Aerospace Science and Technology*, Vol. 45, 2015, pp. 17–29.

[12] Du, X., Venigella, P. K., and Liu, D., "Robust Mechanism Synthesis with Random and Interval Variables," *Mechanism and Machine Theory*, Vol. 44, No. 7, 2009, pp. 1321–1337.

[13] Shafer, G., *A Mathematical Theory of Evidence*, Princeton University Press, 1976.

[14] Zadeh, L., "Fuzzy Sets as a Basis For A Theory of Possibility," *Fuzzy Sets and Systems*, Vol. 1, 1978, pp. 3–28.

[15] Bertsimas, D., Brown, D. B., and Caramanis, C., "Theory and Applications of Robust Optimization," *SIAM Review*, Vol. 53, No. 3, 2011, pp. 464–501.

[16] Ben-Tal, A. and Nemirovski, A., "Robust Convex Optimization," *Mathematics of Operations Research*, Vol. 23, No. 4, 1998, pp. 769–805.

[17] Shapiro, A., Dentcheva, D., and Ruszczynski, A., *Lectures on Stochastic Programming: Modeling and Theory*, SIAM, 2009.

[18] Artzner, P., Delbaen, F., Eber, J.-M., and Heath, D., "Coherent Measures of Risk," *Mathematical Finance*, Vol. 9, No. 3, 1999, pp. 203–228.

[19] Dodson, M. and Parks, G. T., "Robust Aerodynamic Design Optimization Using Polynomial Chaos," *Journal of Aircraft*, Vol. 46, No. 2, 2009, pp. 635–646.

[20] Keane, A. J., "Comparison of Several Optimization Strategies for Robust Turbine Blade Design," *Journal of Propulsion and Power*, Vol. 25, No. 5, 2009, pp. 1092–1099.

[21] Park, G.-J., Lee, T.-H., Lee, K. H., and Hwang, K.-H., "Robust Design: An Overview," *AIAA Journal*, Vol. 44, No. 1, 2006, pp. 181–191.

[22] Padulo, M., Campobasso, M. S., and Guenov, M. D., "Novel Uncertainty Propagation Method for Robust Aerodynamic Design," *AIAA Journal*, Vol. 49, No. 3, 2011, pp. 530–543.

[23] Zaman, K., McDonald, M., Mahadevan, S., and Green, L., "Robustness-Based Design Optimization under Data Uncertainty," *Structural and Multidisciplinary Optimization*, Vol. 44, No. 2, 2011, pp. 183–197.

[24] Lee, S. W. and Kwon, O. J., "Robust Airfoil Shape Optimization Using Design for Six Sigma," *Journal of Aircraft*, Vol. 43, No. 3, 2006, pp. 4–7.

[25] Ryan, K. M., Lewis, M. J., and Yu, K. H., "Comparison of Robust Optimization Methods Applied to Hypersonic Vehicle Design," *Journal of Aircraft*, Vol. 52, No. 5, 2015, pp. 1510–1523.

[26] Levy, H., *Stochastic Dominance, Investment Decision Making Under Uncertainty*, Springer, 2015.

[27] Cook, L. W. and Jarrett, J. P., "Horsetail Matching: A Flexible Approach to Optimization Under Uncertainty," *Engineering Optimization*, 2017.

[28] Anderson, T. W., "On the Distribution of the Two-Sample Cramér-von Mises Criterion," *The Annals of Mathematical Statistics*, Vol. 33, No. 3, 1962, pp. 1148–1159.

[29] Seshadri, P., Constantine, P., Icacarino, G., and Parks, G., "A Density-Matching Approach for Optimization Under Uncertainty," *Computer Methods in Applied Mechanics and Engineering*, 2016.

[30] Scott, *Multivariate Density Estimation: Theory, Practice, and Visualization*, 1992.

[31] Jameson, A., Martinelli, L., and Pierce, N. A., "Optimum Aerodynamic Design Using the Navier-Stokes Equations," *Theoretical and Computational Fluid Dynamics*, Vol. 10, No. 1-4, 1998, pp. 213–237.

[32] Choi, S.-K., Grandhi, R. V., Canfield, R. A., and Pettit, C. L., "Polynomial Chaos Expansion with Latin Hypercube Sampling for Estimating Response Variability," *AIAA Journal*, Vol. 42, No. 6, 2004, pp. 1191–1198.

[33] Li, X., Nair, P. B., Zhang, Z., Gao, L., and Gao, C., "Aircraft Robust Trajectory Optimization Using Nonintrusive Polynomial Chaos," *Journal of Aircraft*, Vol. 51, No. 5, 2014, pp. 1592–1603.

[34] Bichon, B. J., Eldred, M. S., Mahadevan, S., and McFarland, J. M., "Efficient Global Surrogate Modeling for Reliability-Based Design Optimization," *Journal of Mechanical Design*, Vol. 135, 2012.

[35] Johnson, S. G., "The NLopt Nonlinear-Optimization Package," *http://ab-initio.mit.edu/nlopt*.

[36] Gray, J., Moore, K., and Naylor, B., "OpenMDAO: An Open Source Framework for Multidisciplinary Analysis and Optimization," *13th AIAA/ISSMO Multidisciplinary Analysis Optimization Conference*, 2010.

[37] Sethi, S. and Striz, A., "On using the Kreisselmeier-Steinhauser function in simultaneous analysis and design," *Collection of Technical Papers - AIAA/ASME/ASCE/AHS/ASC Structures, Structural Dynamics and Materials Conference*, Vol. 2, 1997, pp. 1357–1365.

[38] Palacios, F., Colonno, M. R., Aranake, A. C., Campos, A., Copeland, S. R., Economon, T. D., Lonkar, A. K., Lukaczyk, T. W., Taylor, T. W. R., and Alonso, J. J., "Stanford University Unstructured (SU2): An open-source integrated computational environment for multi-physics simulation and design," *51st AIAA Aerospace Sciences Meeting*, , No. January, 2013, pp. 1–60.

[39] Palacios, F., Economon, T. D., Aranake, A. C., Copeland, S. R., Lonkar, A. K., Lukaczyk, T. W., Manosalvas, D. E., Naik, K. R., Padron, A. S., Tracey, B., Variyar, A., and Alonso, J. J., "Stanford University Unstructured (SU2): Open-source Analysis and Design Technology for Turbulent Flows," *AIAA Journal*, Vol. 51, No. January, 2014, pp. 1–19.